

Article

Long-Term Simulated Direct N₂O Emissions from German Oilseed Rape Cultivation below the IPCC Emission Factor

Thomas Rübiger, Dorothee Neukam , Astrid Knieß, Ulf Böttcher , Henning Kage  and Insa Kühling* 

Institute of Crop Science and Plant Breeding, Agronomy and Crop Science, Kiel University, Hermann-Rodewald-Strasse 9, 24118 Kiel, Germany; kage@pflanzenbau.uni-kiel.de (H.K.)

* Correspondence: kuehling@pflanzenbau.uni-kiel.de

Abstract: The low nitrogen (N)-use efficiency of intensive winter oilseed rape (WOSR) cropping systems may cause negative environmental impacts, especially due to N leaching and gaseous losses. The aim of this study was to use data from field experiments (five sites across Germany representing typical WOSR regions) for parametrization of a nitrous oxide (N₂O) emission component for implementation into a process-based dynamic plant-soil-atmosphere model (PSAM). After calibration and evaluation with three years of field data from five different N fertilizer treatments, a long-term simulation with 25-year historical weather data was conducted to derive functional relations and emission factors (EFs). The model performed best at higher aggregation levels (cumulative emissions over the entire cropping period, R² of 0.48/0.77 for calibration/evaluation), but also reasonably simulated short-term dynamics (e.g., fertilizer applications, extreme weather events). Site-specific and year-specific N₂O emissions varied within the range of medians from 0.56–4.93 kg N₂O-N ha⁻¹. Mineral fertilizer-induced EFs at economic optimal N inputs ranged from 0.16–0.65%, which was markedly below the aggregated IPCC standard value of 1% for direct N₂O emissions. Generally, the simulated emissions were consistently higher with finer soil textures and increasing N inputs. The process-based approach, moreover, allowed the identification of the major source of N₂O, which mainly originated from nitrification processes.

Keywords: nitrous oxide; GHG emissions; winter canola; simulation; N efficiency; climate change



Citation: Rübiger, T.; Neukam, D.; Knieß, A.; Böttcher, U.; Kage, H.; Kühling, I. Long-Term Simulated Direct N₂O Emissions from German Oilseed Rape Cultivation below the IPCC Emission Factor. *Agriculture* **2024**, *14*, 70. <https://doi.org/10.3390/agriculture14010070>

Academic Editors: Klára Pokovai and Sándor Molnár

Received: 29 November 2023

Revised: 25 December 2023

Accepted: 27 December 2023

Published: 29 December 2023



Copyright: © 2023 by the authors. Licensee MDPI, Basel, Switzerland. This article is an open access article distributed under the terms and conditions of the Creative Commons Attribution (CC BY) license (<https://creativecommons.org/licenses/by/4.0/>).

1. Introduction

Nitrous oxide (N₂O) is one of the most important greenhouse gases (GHGs) contributing to climate change, with a 100-year time horizon global-warming potential 273 times greater than that of CO₂ [1]. Fifty-two percent of the anthropogenic direct N₂O emissions are caused by agriculture and 58% of the natural global annual N₂O emissions are from soils [2]. To prevent further global warming, emissions of N₂O must be urgently reduced. Therefore, process-based dynamic crop models can help to better understand relevant processes and to identify priorities.

The complex interactions of many soil, microbial, and plant nitrogen (N)-associated processes (volatilization, leaching, mineralization, nitrification, denitrification, immobilization, plant N uptake, litter production) at varying spatial and temporal scales make this a challenging task. The microbial processes of nitrification and denitrification are the most important processes for N₂O formation from soils [3–5]. Nitrifiers perform the exothermic oxidation of ammonium (NH₄⁺) to nitrite and nitrate. These processes depend on soil NH₄ content, soil water content, pH value, and soil temperature [6,7]. Denitrification is the heterotrophic, successive reduction of nitrate (NO₃⁻) to nitrite (NO₂⁻), nitric oxide (NO), nitrous oxide (N₂O), and dinitrogen (N₂) by a large community of microbes [8,9]. These processes are also influenced by the oxygen concentration in the soil, the soil temperature, the pH value and the concentrations of the substrates NO₃⁻ and microbial available carbon (C) [7,8,10,11]. The NO₃ concentration depends on the availability of reactive nitrogen

(defined as organically bound N and inorganic N, except N_2) and is a key factor triggering N_2O soil emissions [7]. The oxygen availability for the soil microbes is mainly influenced by the volumetric soil water content [10], the oxygen consumption of the soil microbiota itself, and plant roots. Increasing soil temperatures stimulates microbial activity and the related oxygen consumption by the microbiome [7]. Therefore, N_2O emission peaks under nearly water-saturated conditions and sharply decreases when the soil becomes drier [12]. Maximum N_2O emissions occur at values of around 80% water-filled pore space (WFPS) [7]. At WFPS higher than 80%, nitrification is inhibited and denitrification turns to the most important N_2O source [13].

Soil-derived N_2O emissions are commonly measured using closed chambers, but these measurements are time-consuming, expensive, and, therefore, limited [14]. Simulation models are an option to extrapolate N_2O emissions to various temporal and spatial scales and to analyze sensitivities to environmental and management factors [15–17]. To calculate GHG balances on national and continental scales, the Intergovernmental Panel on Climate Change (IPCC) recommended a simple empirical emission-factor approach as a robust tool to estimate annual N_2O emissions associated with agricultural practices and land-use change [18]. The linear IPCC Tier 1 emission factor (EF) assumes that 1% of the total N input by fertilizers and N in crop residues is emitted directly as N_2O [19]. However, as N_2O emissions from crop production depend on many site-specific agricultural practices like fertilization, tillage, and residue management [16], such linear Tier 1 approaches are limited. A global meta-analysis revealed a general non-linear response of N_2O emissions to N fertilizer [20]. Improvements from Tier 1 replacement by stratified European EFs better reflected spatial variability [21]. Ruser et al. [22] specifically showed that fertilizer-related N_2O emissions for WOSR cultivation are not linear and that WOSR-specific EFs are often markedly lower than 1% in Germany. They also emphasized substantial spatio-temporal variation. Mathivanan et al. [23] recently evaluated a Tier 2 regionalization of EFs across Germany, resulting in an average EF of 0.62% (range: 0.38–0.92%), which was markedly below the Tier 1 standard value.

Beyond such Tier 2 approaches, dynamic process-based simulation models allow for the calculation of N_2O emissions as a result of different simultaneously occurring N turnover processes [7]. These kinds of models have been proven to be useful for field-scale simulation and analysis of N_2O emissions [24] and are requested for future climate inventories under a Tier 3 approach. They further allow causal analysis of processes and driving forces, as well as site-specific scenario calculations. However, a reasonably good simulation of N_2O emissions over a range of environmental and management conditions is still challenging. These difficulties arise at least partly from the challenge that processes influencing the boundary conditions need to be properly covered. Thus, an N_2O emission model should be integrated into a well-performing, process-oriented plant-soil-atmosphere model (PSAM) under the given pedoclimatic conditions.

The aim of this study was to (i) develop and parametrize a model component for N_2O emissions for integration into an existing PSAM model suitable for high-yielding conditions of WOSR cultivation, for simulation of daily and cumulative fluxes. Subsequently, the model was subjected to a site- and fertilizer-specific (ii) calibration and (iii) evaluation with independent observations. Furthermore, (iv) generalized site-specific EFs for varying N fertilizer input based on long-term weather data were derived.

2. Materials and Methods

2.1. Experimental Sites and Field Trials

In 2012, field trials with identical crop rotation winter oilseed rape (WOSR)-winter wheat-winter barley were established at five sites across Germany, as a completely randomized block design with four replications. The studied sites represented typical regions with high yields and acreage of WOSR under differing pedoclimatic conditions (Figure 1, Tables 1 and 2).

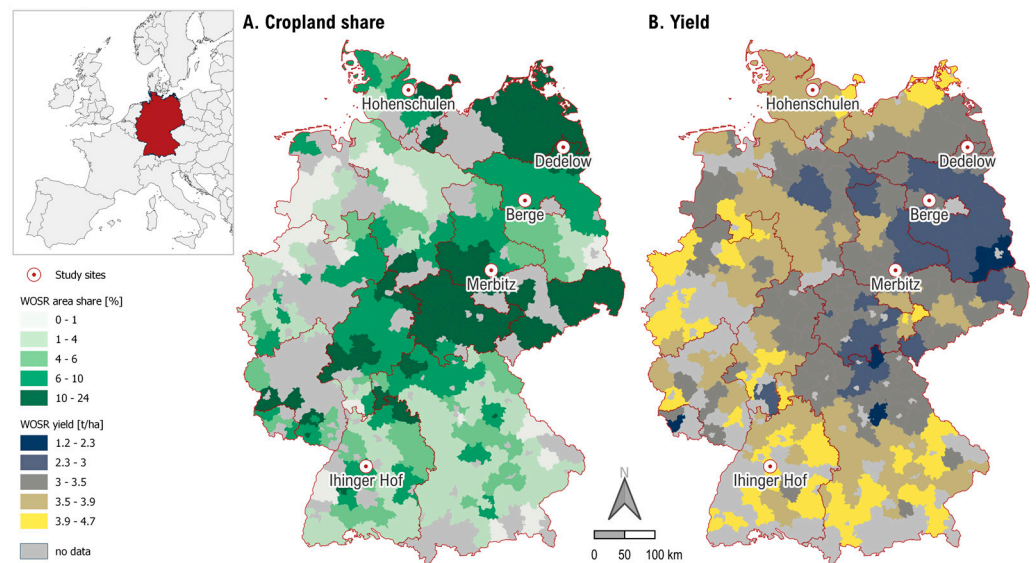


Figure 1. Location of the five study sites in regions with a high winter oilseed rape (WOSR) cropland share (mean 2010–2020) and different yield levels (mean 2018–2022). Data source: [25].

Table 1. Soil conditions of the study sites after IUSS classification.

Site	Soil Type [IUSS]	Clay [%]	Silt [%]	Sand [%]	Texture Class [IUSS]	pH	Corg [%]	Nt [%]
Berge	Luvisol	9.3	18.5	72.2	SaLo	6.5	1.15	0.09
Dedelow	Luvisol	10	30.9	59.1	Lo	7.4	0.75	0.10
Hohenschulen	Haplic Luvisol	10.5	29.4	60.1	Lo	6.0	1.68	0.20
Ihinger Hof	Haplic Luvisol/Anthrosol	3.2	78.2	18.6	SiLo	6.8	1.87	0.12
Merbitz	Haplic Chernosem	15.8	67.8	16.4	SiCILo	6.6	1.18	0.11

Table 2. Annual mean temperature and precipitation sum of the three experimental years together with their long-term average (LTA).

Site	[°C]	Temperature			[mm]	Precipitation		
		Yearly Deviation [°C]	Yearly Deviation [mm]					
	LTA	2013	2014	2015	LTA	2013	2014	2015
Berge	8.7	+0.7	+4.3	+1.9	503	+112	−21	+67
Dedelow	8.4	+0.3	+1.5	+1.3	485	−39	+76	−71
Hohenschulen	8.9	−0.8	+0.8	−0.1	732	−78	−323	+38
Ihinger Hof	8.3	+0.4	+2.2	+1.8	688	+235	+75	−144
Merbitz	9.0	+0.1	+1.7	+1.4	520	+180	−64	−91

Within this study, we only focused on data and simulations for the WOSR cropping period and succeeding wheat until spring fertilization. Winter oilseed rape was sown at densities of 40–45 plants m^{-2} between the end of August and mid-September. Five N treatments were tested: 0 N (unfertilized control), 120 CAN (60 + 60 kg N ha^{-1} as calcium ammonium nitrate (CAN), 27% N), 180 CAN (90 + 90 kg N ha^{-1}), 240 CAN (120 + 120 kg N ha^{-1}), and 180 DIG (90 + 90 kg NH_4-N ha^{-1} as biogas digestate (DIG)). Mineral N was applied at the beginning of spring growth and at stem elongation. All other nutrients were site-specifically applied according to regional farmers' practices, and further crop management was conducted uniformly according to best-practice recommendations for all N treatments. More details about the exact yearly dates for sowing and fertilization and digestate characteristics are presented in the Supplementary Materials.

2.2. Field Data Collection

Soil mineral nitrogen (SMN) and soil moisture in 0–30 cm depth were sampled weekly as the sum of $\text{NH}_4\text{-N}$ and $\text{NO}_3\text{-N}$. Soil moisture was quantified gravimetrically from subsamples. At each field research station, a meteorological station delivered daily weather data.

The field measurements and the flux calculations of N_2O were described in detail by Ruser et al. [22]. In brief, non-steady-state chambers were used to estimate gas fluxes at least weekly in the row interspace of WOSR and within the winter wheat crops. During a maximal closure time of one hour, four gas samples were taken every 20 min using a syringe, transferred into glass exetainers, and then analyzed gas-chromatographically for N_2O concentrations. Fluxes were calculated using the R package gasfluxes [26], a procedure combining non-linear and robust linear flux models. After a rigorous quality check [22], N_2O fluxes were linearly interpolated between weekly sampling dates. Monthly and annual N_2O emissions were derived by cumulating interpolated daily fluxes for further model-performance analytics.

2.3. Model Description

Based on existing approaches, a newly tailored conceptual N_2O -emission model component was developed for integration into an existing plant-soil-atmosphere model (PSAM) [27]. The previously well-evaluated process-based PSAM combines submodules for the dynamic simulation of crop growth, N uptake of WOSR (HUME-OSR: [28,29]) and winter wheat (HUME-Wheat: [30]), evapotranspiration, soil water and NO_3 transport, mineralization, and management events on daily timesteps with weather data as external driving forces. All submodules were implemented in the HUME modeling environment [31,32].

2.3.1. Structure of the N_2O Model Component

The N_2O -emission model calculates total N_2O emissions as the sum of N_2O emission rates derived from nitrification and denitrification (Figure 2). Nitrification of ammonium was simulated as a first-order kinetic process that depends on the NH_4 pool and the nitrification rate (Equation (1)). Therefore, the potential nitrification rate k_{nit} was reduced by an abiotic factor $f_{abiot_{nit}}$ corresponding to the effect of soil temperature and soil water [33,34]. According to the ratio of NO_x and N_2O $R_{\text{NO}_x/\text{N}_2\text{O}}$, emissions from nitrification N_2O_{nit} were then derived from the gaseous N loss, calculated by using an N-loss fraction factor fr_{n-loss} :

$$\text{N}_2\text{O}_{nit} = k_{nit} \cdot f_{abiot_{nit}} \cdot \text{NH}_4 \cdot fr_{n-loss} \cdot \frac{1}{1 + R_{\text{NO}_x/\text{N}_2\text{O}}} \tag{1}$$

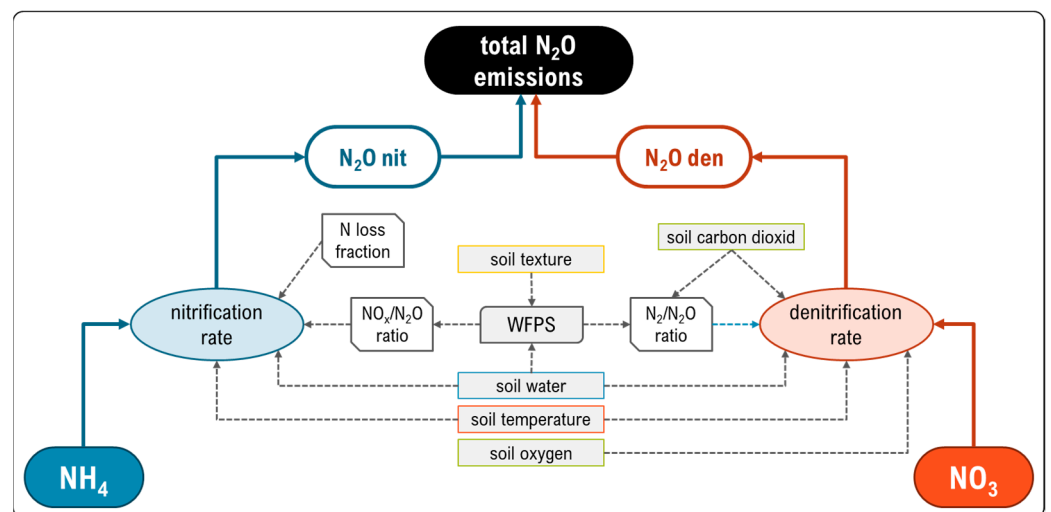


Figure 2. Schematic overview of the N_2O -emission underlying processes and driving forces.

The abiotic factor $f_{abiot_{nit}}$ was calculated from soil water and temperature impacts according to Hansen et al. [34], based on Equations (A1)–(A3) (see Appendix A for details). The ratio of NO_x and N_2O decreased with increasing water-filled pore space (WFPS) [33], according to Equation (A4).

Denitrification of NO_3 was calculated from a potential denitrification rate $k_{pot_{den}}$ and reduction functions $f_{abiot_{den}}$ for soil temperature, soil water, and oxygen status, according to the APSIM model [35] (Equation (2)). NO_3 availability further reduced the denitrification rate based on a Michaelis-Menten kinetics approach, as recommended by Heinen [24]. N_2O emission from denitrification N_2O_{den} was calculated as follows:

$$N_2O_{den} = k_{pot_{den}} \cdot \frac{NO_3}{K_m + NO_3} \cdot f_{abiot_{den}} \cdot \frac{1}{1 + R_{N_2/N_2O}} \quad (2)$$

where K_m is the Michaelis constant, $f_{abiot_{den}}$ is the correction factor for abiotic impacts, and R_{N_2/N_2O} is the ratio of N_2 and N_2O .

The potential denitrification rate $k_{pot_{den}}$ is related to the CO_2 -flux from soil respiration during mineralization as proxy for available organic substrate, using a fit parameter k_{den} [34], according to Equation (A5). The abiotic correction factor $f_{abiot_{den}}$ is the product of factors representing the effect of water and temperature (Equation (A6)). Denitrification only occurs if soil water conditions exceed a critical WFPS (Equations (A7) and (A8)). The temperature impact was calculated according to the APSIM model of Thorburn et al. [35], based on Equation (A9). The ratio of N_2 and N_2O correlated positively with both water-filled pore space WFPS [$\text{cm}^3 \text{ cm}^{-3}$] and the CO_2 emission rate [$\text{kg C ha}^{-1} \text{ d}^{-1}$], but decreased with the increasing nitrate amount NO_3 [kg N ha^{-1}], according to Del Grosso et al. [36] (for intact soils, following Equations (A10)–(A12)).

2.3.2. Model Initialization and Parametrization

The existing PSAM, with calibrated and evaluated soil water and N processes [27], was further adapted for implementation of the N_2O dynamics. At first, parameters describing the soil water retention curve and the unsaturated hydraulic conductivity [37] were deduced from the soil textures. Then, the mineralization parameters were manually fitted to observed SMN dynamics, adjusting the turnover rates for soil organic matter ($k_{SOM \rightarrow BIOM}$) and the tillage effect (Min_{eff} ; following Henke et al. [38]). Further turnover rates were taken from Hansen et al. [34]. C/N ratios of the four coupled carbon pools: soil organic matter (SOM), decomposable plant material (DPM), resistant plant material (RPM), and microbial biomass (BIOM) and corresponding microbial substrate use efficiencies (ϵ)—were adopted from Verberne et al. [39]. The different management events like sowing, fertilization, and harvest date were also considered. Subsequently, the N_2O data and the driving forces for both nitrification and denitrification were used for parameterization of the N_2O emission model, i.e., adjusting the fraction of N loss during nitrification ($fr_{Nloss_{nit}}$) and the fit parameter (k_{den}) scaling the CO_2 flux to potential denitrification. Furthermore, $WFPS_{crit_{den}}$ was adjusted site-specifically to meet measured N_2O (Table A1).

Each model run started after the harvest of the preceding crop (July) before WOSR establishment and ceased at the beginning of spring growth of the subsequent wheat crop (March) after WOSR harvest (Σ 21 months) in order to simulate the entire period of WOSR-related N_2O emissions being measured. For model initialization, site-specific soil data (bulk density, organic C and N content, and soil texture) were used. Initial SMN and soil water content were adapted to meet first-measured values. Daily weather data (precipitation, air temperature, humidity, global radiation, and wind speed) from the field weather stations next to the five studied sites were used as external drivers.

2.3.3. Model Calibration and Evaluation

For independent model calibration and evaluation, the data were divided into two subsets. For each site, measured N_2O -emission data from the treatments 0 N, 180 CAN, and 180 DIG were used, together with complementary data such as SMN, soil water content at

0–30 cm and N uptake of WOSR during model calibration. Thereafter, the parametrized model was tested, without further adaptations, against the remaining observation data of two other treatments (120 CAN and 240 CAN) that were not used during the calibration for independent model evaluation. This procedure was carried out identically for all sites. Model performance was evaluated based on linear regressions of simulated over measured data (intercept, slope, and R^2) and root mean square errors (RMSEs). All calculations were carried out in R [40].

2.4. Long-Term Simulations

To estimate generalized site-specific annual N_2O -emission amounts for each studied fertilizer treatment under various climatic conditions, long-term simulations were conducted by model runs with site-specific long-time weather data (1991–2016; German Weather Service). To determine mean dates of specific management events (for tillage, sowing, fertilization, and harvest), site-specific averages of the three investigated years were assumed for each management event. For comparability, the properties of the organic fertilizer (DIG treatment) were regarded as the same for all sites in all years, by averaging across all environments in these 25-year simulations. NH_3 losses of the digestates were considered site-specifically, as determined by Rübiger et al. [27]. A 21-month period was calculated for each simulation run, subdivided into six months of warm-up to ensure realistic volumetric water contents and SMN amounts followed by 15 months as a potential balancing period. N_2O emissions were then cumulated from 1 January to 31 December, to be comparable to other findings.

2.5. N-Input Sensitivity Analysis and Emission-Factor Calculation

The response of annual direct N_2O emissions to fertilizer N input (continuously increased from 0–300 kg N ha^{-1}) was investigated in a sensitivity analysis. Functional relations of N input and N_2O emissions could be derived from these modelings. The simulation duration per run and the balancing period for direct N_2O emissions were the same as for the long-term simulation with 25 years of weather data. Finally, site-specific fertilizer-induced emission factors (EFs) were calculated from the derived functional relations, as follows:

$$EF [\%] = ((E_i - E_0) / i) \cdot 100 \quad (3)$$

where E_0 and E_i are predicted annual emissions [kg N $ha^{-1} a^{-1}$] at 0 and i kg N fertilizer amounts (representing background emissions), respectively. To compare the sites at the same N level, $i = 200$ kg N was chosen. Additionally, the EF at economically optimal N input ($EF_{N_{opt}}$) was calculated for each site. Economically optimal N (N_{opt}) was defined as the N fertilizer input with maximum economic gross margins [41,42]. It was determined from site-specific quadratic N-response functions, assuming 0.8 € kg^{-1} N fertilizer and 360 € t^{-1} WOSR seed.

3. Results

3.1. Dynamics of Daily N_2O Fluxes

Based on N_2O measurements from five sites over three years, the capability of the model to predict daily and cumulative N_2O emissions on a monthly basis, or over the entire period, was tested. Regarding the site-specific magnitude and temporal dynamics, the model generally reproduced the observed daily N_2O emissions in an acceptable way (Figures 3 and 4). It simulated spring peak emissions after fertilizer applications, as well as unfertilized control treatments, and correctly predicted low emission rates during dry periods. However, some of the simulated daily N_2O emissions differed remarkably from the measured values.

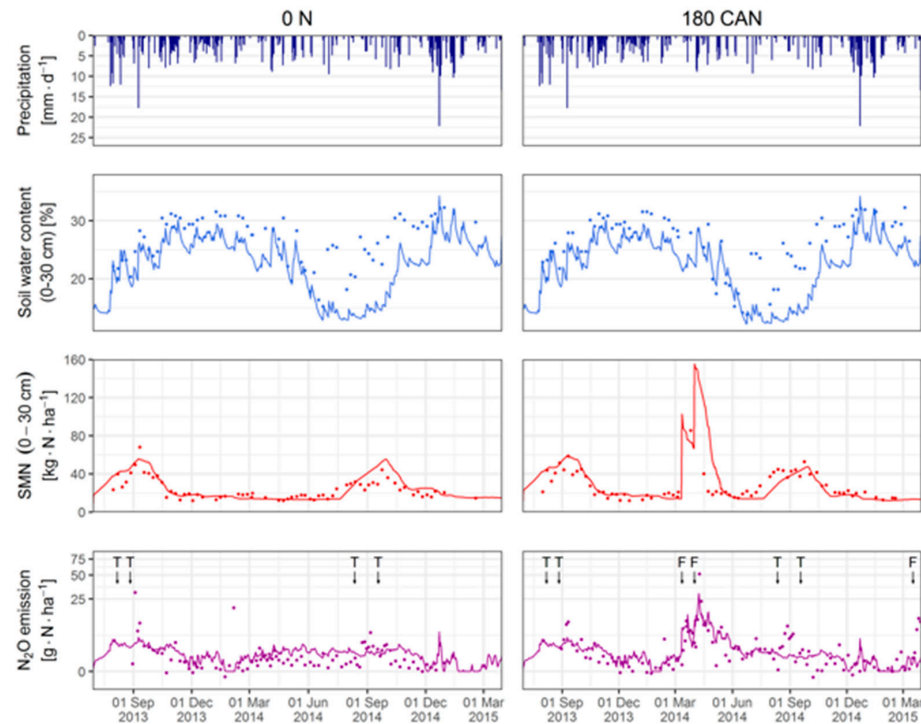


Figure 3. Exemplary simulated (lines) and observed (points) dynamics of soil water content, soil mineral nitrogen (SMN), and N_2O emissions, as well as precipitation, in daily time steps for the treatments without N input (0 N) and with typical N input (180 CAN) at the Hohenschulen site for the oilseed rape harvest year 2014. T: tillage event; F: fertilization event; the y axis of daily N_2O flux was scaled using log-modulus transformation.

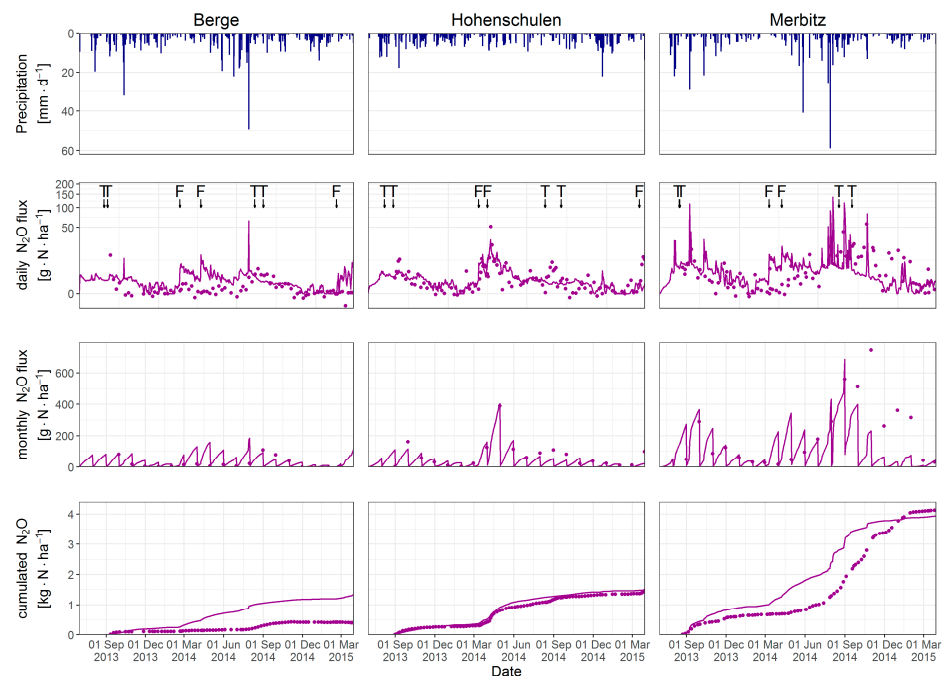


Figure 4. Exemplary comparison of site-specific N_2O emissions on three levels of aggregation (daily, monthly, and cumulated over the entire measuring period) for the treatment with 180 kg mineral N application from calcium ammonium nitrate (CAN) at three selected sites, indicating low-, medium-, and high-emission conditions. Measured data are shown as points, simulated values are shown as lines. Harvest year of oilseed rape: 2014; T: tillage event; F: fertilization event; y axis of daily N_2O flux was scaled using log-modulus transformation.

For instance, the simulation of N_2O emission peaks that occurred after tillage events and the increased post-harvest emissions from WOSR residues at the Hohenschulen site failed (Figure 3). Contrary, high N_2O peaks were simulated after heavy rain events that were not covered by field measurements (Figure 4: daily N_2O fluxes at Berge and Merbitz). Furthermore, the observed increase of SMN after tillage was reproduced by the model, as well as the increasing SMN after fertilization events, as shown for Hohenschulen in Figure 3. Generally, the simulation of SMN for all sites and years showed plausible dynamics as necessary for an important driving factor of gaseous N losses (for details of soil-water-nitrogen dynamics, please refer to [27]).

3.2. Cumulative N_2O Emissions

Site-specific N_2O emissions on three levels of temporal aggregation are shown in Figure 4 for the treatment 180 CAN in 2014 at Berge, Hohenschulen, and Merbitz, representing low-emission, moderate-emission, and high emission sites within our study (according to Ruser et al. [22]). Although the values of statistical criteria (Table 3) showed that, at all sites, daily simulated N_2O emission hardly matched the observations after model calibration, the monthly aggregated values were more consistent with measured values in terms of magnitude and pattern, resulting in an acceptable goodness of fit for cumulated N_2O emissions during the observed periods. Generally, the simulations slightly overestimated cumulated N_2O emissions, especially at Ihinger Hof, Dedelow, and Berge (Figure 5A). Nevertheless, the model was able to reproduce site-specific patterns and differences in N_2O emissions and sources after calibration (Figure 6).

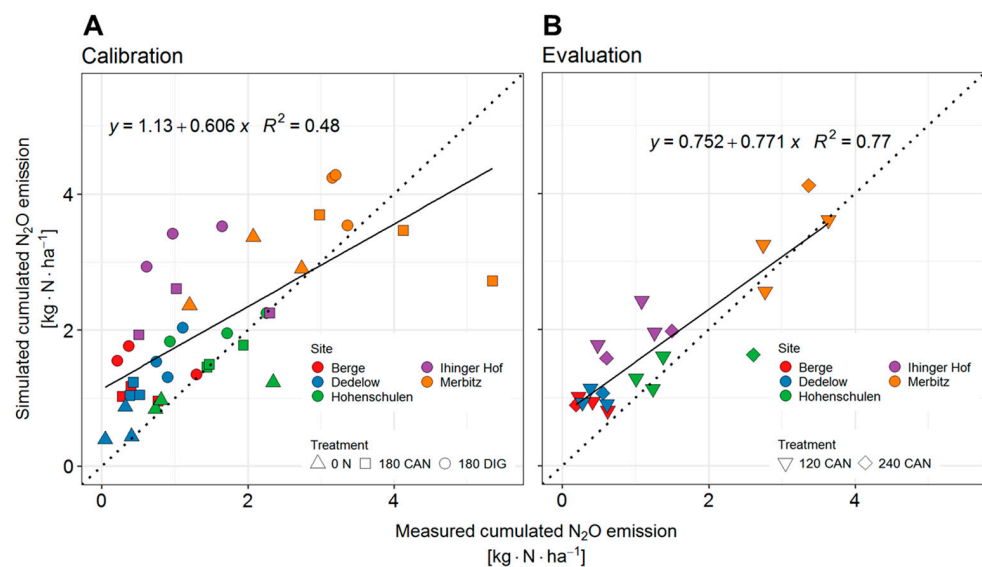


Figure 5. Comparison of measured and simulated cumulated N_2O emissions for the five sites and the three periods (>12 months) for both calibration data ((A): $n = 39$; $RMSE = 1.05 \text{ kg N ha}^{-1}$) and evaluation data ((B): $n = 21$; $RMSE = 0.69 \text{ kg N ha}^{-1}$).

Organic fertilization (DIG) resulted in higher means of cumulated emissions compared to the mineral treatments (Figure 5A). A comparison of the goodness of fit for calibration and evaluation data revealed the capability of our model to simulate cumulated N_2O emissions reasonably for the five sites without further re-parametrization (Figure 5B).

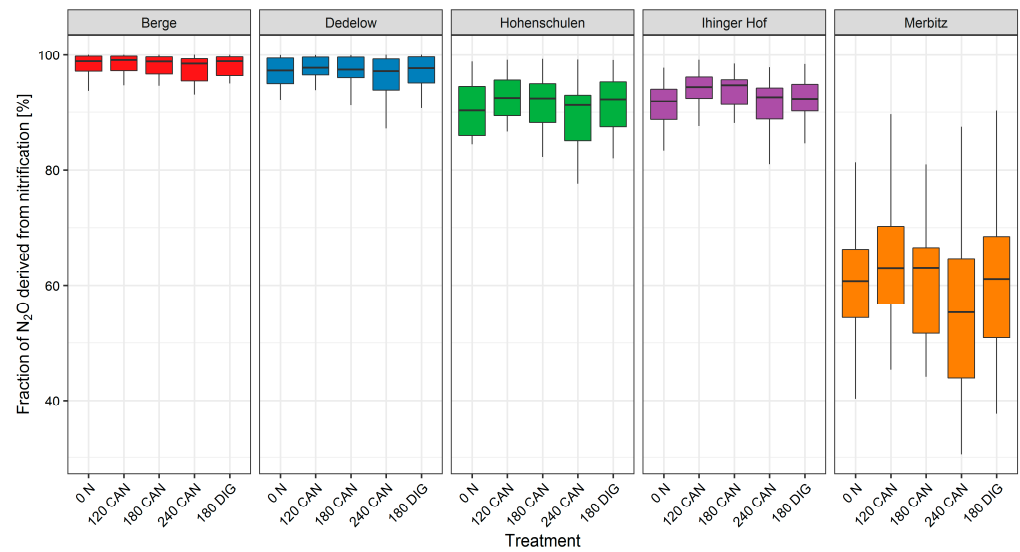


Figure 6. Simulated fraction of yearly N_2O -emissions from nitrification relative to total emissions for all sites and N treatments ($kg\ ha^{-1}$ N input; CAN: calcium ammonium nitrate, DIG: biogas digestate with $kg\ NH_4-N$).

Table 3. Statistical criteria for simulated and measured N_2O emissions for the calibration and evaluation dataset. Statistics are provided for the entire simulation period (total), monthly periods, and daily periods of simulated vs. measured N_2O -emissions.

Dataset	Calibration			Evaluation		
	total	monthly	daily	total	monthly	daily
Aggregation level	total	monthly	daily	total	monthly	daily
No. of observations	39	604	2228	21	304	1144
R^2	0.48	0.23	0.065	0.77	0.34	0.064
Slope	0.606	0.41	0.16	0.771	0.53	0.12
Intercept	−1.13	0.09	0.004	0.752	0.07	0.004
RMSE [$kg\ N\ ha^{-1}$]	1.05	0.17	0.01	0.69	0.13	0.01

3.3. Long-Term Simulated Mean Annual Emissions

The long-term simulation over 25 years showed site-specific N_2O emissions varying between sites and years within the range of medians from 0.56 – $4.93\ kg\ N_2O-N\ ha^{-1}$ (Figure 7). Generally, emissions increased with increasing N input and were highest for the organic treatment at each site. The emission level was lowest at Berge, while Merbitz showed the highest values. At Berge and Hohenschulen, the emission values of the three investigated years were almost within the interquartile range of the simulation study, meaning that they represented average years. The same applied for Merbitz, except for the organic treatment, where the interquartile range of calculated annual emissions exceeded the measured values of all three years. At Ihinger Hof and Dedelow, the measured N_2O emissions were partly below the median level of the long-term simulation, especially in 2015. At Merbitz, the N_2O emission levels across all N treatments were the highest, with markedly larger variation, compared to all other sites (Figure 7).

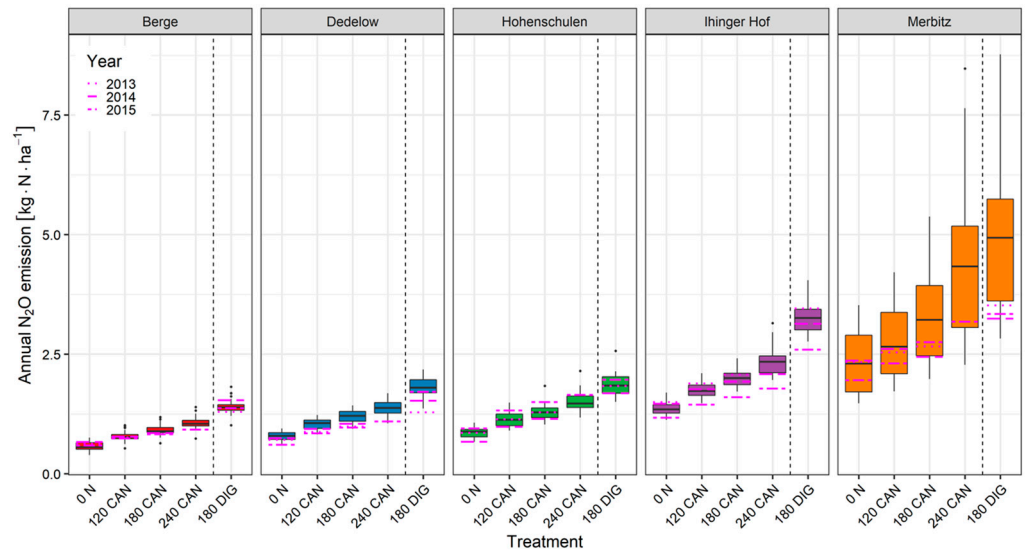


Figure 7. Simulated long-term annual levels (1991–2016) of N₂O emission of the five study sites and the fertilizer treatments (boxplots) and corresponding simulated values of the three experimental periods (horizontal lines, 2013–2015); CAN = kg N from calcium ammonium nitrate, 180 DIG = 180 kg NH₄-N + organic N.

3.4. Fertilizer Related Emission Factors

Furthermore, the conducted long-term simulations for all study sites enabled a sensitivity analysis of continuously increased N fertilizer input between 0 and 300 kg N ha⁻¹. Direct N₂O emissions as functions of mineral N input showed a rather non-linear response and were considerably lower than the IPCC standard calculations (Figure 8). Only at the high-emitting Merbitz site, emissions above the economic optimum N input > 200 kg N ha⁻¹ yr⁻¹ reached the IPCC level in a few years of the long-term simulation. The median level exceeded 1% only at a fertilization level > 280 kg N ha⁻¹ yr⁻¹, which was far beyond agricultural practice. At all other sites, maximum simulated emissions were also markedly below the IPCC range for all of the considered N fertilizer inputs.

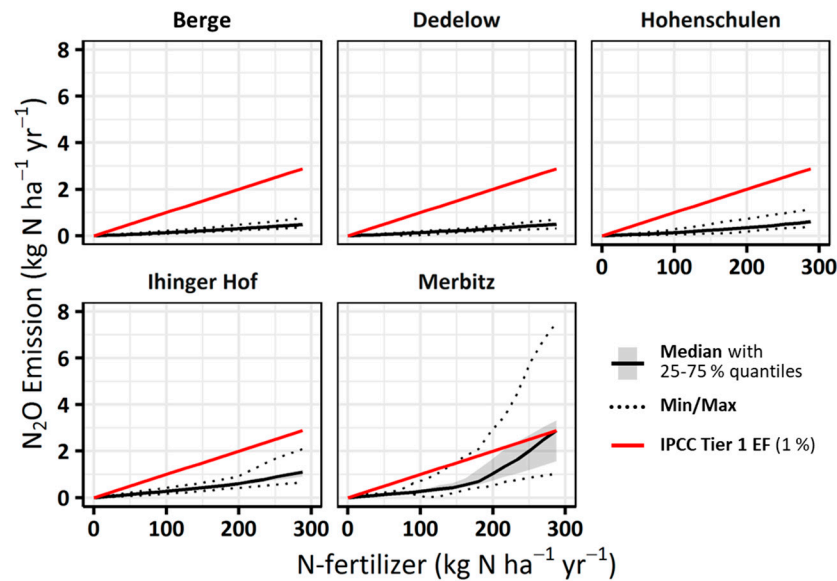


Figure 8. Simulated annual long-term N₂O emissions of the five sites as a function of mineral N fertilization, in contrast to emissions calculated by the linear IPCC default emission factor (EF).

Based on these results, functional relations between N input and annual direct N₂O emission could be successfully fitted from nonlinear functions (second-order polynomials) with coefficients of determination between 0.61 and 0.90 (Table A2). Based on those equations, fertilizer-related EFs were calculated for each site, based on Equation 3, for selected N-input levels (Table 4).

Table 4. Mean emission factors (EFs) for selected N input levels (200 kg N ha⁻¹, site specific economic optima (N_{opt}) from mineral fertilizer and 180 kg NH₄-N from organic sources (DIG)).

Site	EF200 [%]	EFN _{opt} [%]	EF180 DIG [%]
Berge	0.165	0.164	0.462
Dedelow	0.161	0.161	0.579
Hohenschulen	0.184	0.192	0.542
Ihinger Hof	0.321	0.334	1.050
Merbitz	0.648	0.651	1.419

These representative EFs derived from variable weather conditions during the 25-year long-term simulation, reflecting the positive correlation with the used fertilizer amount. At Berge, Dedelow, Hohenschulen, and Ihinger Hof, all derived EFs were clearly below the IPCC default of 1% (Table 4). Obviously, at sites with potentially high annual emissions, the resulting fertilizer-induced EFs were also high. The EF₂₀₀ increased in the order Dedelow < Berge < Hohenschulen < Ihinger Hof < Merbitz and enabled direct comparability. For site-specific N_{opt} inputs between 191 and 222 kg N ha⁻¹ (Table A3), EF_{N_{opt}} were similar or slightly higher, but also all clearly below the 1% value according to the IPCC.

For the organic treatments, EFs were calculated at the 180 kg DIG ha⁻¹ level (Table 4), based on the results of the simulated long-term annual N₂O emission levels with an average digestate input (Figure 7). Merbitz was the site with the highest organic EF (1.42%); at Ihinger Hof (1.05%), the IPCC factor was slightly exceeded by emissions from digestate. The other study sites were, likewise, around half the aggregated IPCC Tier 1 level for organic N inputs.

4. Discussion

4.1. Driving Forces of N₂O Flux Dynamics

Accurate GHG inventories and identification of regionally-tailored mitigation options should consider the spatial variability of soils and climate [43]. Simulations using process-oriented models are, principally, a suitable approach to address these aspects. However, all relevant driving forces of the N₂O-producing processes, and the processes themselves, must be simulated with acceptable accuracy to obtain more useful results, rather than results from more simple or aggregated approaches [7,44,45].

The amount of SMN, as a source for N₂O-producing microbes, is a key factor influencing N₂O formation and varies substantially. Zhou et al. [33] stated that precise simulation of SNM is a prerequisite for sufficiently accurate N₂O-emission estimates. The used PSAM provided a plausible simulation of SMN dynamics for all N rates, N forms, sites, and years [27]. The time course and the maximum amount of N uptake by the crops and the level of N mineralization from soil organic matter are key processes in order to estimate SMN, and they were properly covered by our PSAM as well [27]. Some N₂O emission-focused models have been reported to sometimes fail in the prediction of crops' N uptake [46], or to miss information about the performance of N-uptake simulation.

Soil moisture is another major driver of N₂O emissions, as it governs the oxygen availability to soil microbes [7,47], in conjunction with soil texture and structure. Soil moisture, therefore, affects both processes—nitrification as well as denitrification—in terms of the total rate and the fraction of N₂O emission to the total gaseous N loss for the respective process. Our model often simulated soil water dynamics well [27], presumably because of the soil water diffusivity-based approach [32], which accounts for the temporal

oversaturation of soil compartments. Usually, this leads to a better description of water-flow rates, compared to tipping-bucket approaches used in other N₂O emission models such as, e.g., DNDC [48].

The critical WFPS for denitrification ($WFPS_{crit_den}$) was introduced as a site-specific factor controlling the start of denitrification as an extension of the original APSIM approach [49] or as used in the process-based ECOSSE model [47]. In contrast to the calibration of nitrification parameters, where no site-specific calibration was required, for denitrification a site-specific calibration of $WFPS_{crit_den}$ substantially improved the estimations of N₂O emissions [43,47]. For all sites in this study, denitrification starts at soil water contents exceeding field capacity, as indicated by site-specifically calibrated $WFPS_{crit_den}$. The difference between $WFPS_{crit_den}$ (ranging from 0.8–0.95) and the WFPS at field capacity was higher for the more sandy soils in Berge, Dedelow, and Hohenschulen. Therefore, the use of a simple cascading-layer approach for simulating soil water dynamics seems to be inappropriate [50]. Although the data (Tables 1 and A1) suggested a correlation between site-specifically calibrated parameters and soil textures, we were not able to establish functional relationships between those two factors. This might indicate that further factors, like soil organic carbon (SOC) content or bulk density, might control mineralization processes and N₂O emissions, especially for the denitrification-driven N₂O fraction.

The results of Thorburn et al. [35] revealed higher N₂O emissions in heavier textured soils, which is in line with our observations at Merbitz, where clay content and the long-term annual N₂O emission levels were highest. Moreover, Groffman and Tiedje [51] reported that the smaller pores of earlier fine-textured soils become anaerobic, favoring denitrification. In contrast, the sandy-soil texture at Berge and Dedelow, with the lowest water-holding capacity, caused only small N₂O emissions [22]. Velthof et al. [52] measured low N₂O emission rates on soil with relatively low organic matter. The lowest SOC concentrations were found at Berge and Dedelow, representing low-emission sites in our experiment. Interestingly, the highest SOC contents were measured at Hohenschulen and Ihinger Hof, while the high-emission Merbitz site showed an intermediate SOC content.

In addition to soil-related parameters, a reliable crop-growth simulation is also important to derive WOSR-specific emission results. The chosen environment of HUME-OSR is known for good predictions of WOSR-yield formation under German conditions [28]. The implementation of allometric partitioning outperformed phenologically driven development in high-yielding environments that are typical in Germany. Therefore, in our study, HUME-OSR as a basic PSAM was superior to the widespread utilized APSIM model under less-intensive production conditions.

4.2. Source Paths of N₂O Emissions

Generally, the used parameterization of the N₂O emission model suggests a predominantly nitrification-driven N₂O development. This is supported by the observations that N₂O emissions peaked after application of fertilizer N (Figure 3) under conditions of only moderate soil water saturation. Furthermore, the model of Li et al. [15] estimated that 68% of total N₂O emissions in the unfertilized control derived from nitrification. Nevertheless, large year-specific and site-specific differences in N₂O composition occurred (Figure 6), as revealed by the share of nitrification of 62% at Merbitz, whereas at all other sites more than 90% of the emitted N₂O was derived from nitrification for long-term medians of the 180 CAN treatment. However, the large boxes and long whiskers of the long-term simulation indicate denitrification as an important source for N₂O formation in certain years at Merbitz, especially for the 240 CAN treatment (Figure 6). As a clear correlation, larger shares of denitrification were simulated in years with higher precipitation.

For the digestate treatment, the share of nitrification was generally slightly higher compared to the highest CAN treatment (Figure 6), probably due to high proportions of NH₄-N (equivalent to 180 kg N ha⁻¹ as CAN) being the N source of nitrifiers. Additionally, the increased O₂ consumption during mineralization of organic-bounded N may have an additional effect on N₂O emission rates. Köster et al. [4] showed that bacterial denitrification

seems to be the main source of N₂O produced after biogas residue application to moist soils. This was due to high amounts of labile carbon feeding denitrifiers and the NO₃ supply by the organic fertilizer. High N₂O peaks, observed shortly after manure application, were ascribed to increasing denitrification rates and triggered by easily degradable organic substrates [52,53]. Our experimental data did not always show those kinds of N₂O peaks shortly after digestate application, but our simulation did so, to some extent, and therefore led to a slight overestimation (Figures 5 and 6).

4.3. Model Purpose and Level of Aggregation

The model provided reasonable estimates of cumulated N₂O emissions for increasing N-input levels at the different sites for the three periods (Figure 5). However, further improvements are needed to explain the short-term variability, which is not well covered by the actual parametrization. Since the field measurements in our study were conducted weekly, it may be possible that some peaks were not recorded, especially in sensitive stages such as after fertilization or precipitation. This lack of experimental data from flux measurements was also mentioned as a reason by Goglio et al. [16], using the CERES-EGC model. A model approach should be able to deduce these sensitive stages and calculate the corresponding N₂O emission, resulting in an overestimation compared to measured data. Otherwise, underestimation could occur within the modeling process due to model errors from erroneous simplifications of real situations. Whereas more complex models like DNDC [54] take anaerobic microsites in the soil into account ('anaerobic balloon'), they were not explicitly covered by our modeling approach. Zhou et al. [33] mentioned both possibilities of overestimation and underestimation by modeling approaches, resulting in discrepancies between daily simulated and measured N₂O emissions.

Even for monthly aggregated emissions, some discrepancies between our simulations and observations still occurred, resulting in global coefficients of determination of 0.23 and 0.34 for calibration and evaluation data sets, respectively (Table 3). These results are in line with the findings of Yang et al. [55] for N₂O modeling with the SWAT model on monthly time steps in corn and switchgrass systems ($R^2 = 0.2253$). Their model performed better ($R^2 = 0.497$) when excluding a month with high N₂O emissions, indicating that single high N₂O peaks can largely affect model performance on monthly time steps.

Our model performed best for cumulated N₂O emissions representing the site-specific amount of N₂O being emitted within the measured period. This is comparable to modeling studies of Bell et al. [56] and Molina-Herrera et al. [57], where cumulated emissions were better met from the models than from daily or weekly measurements. For balancing purposes, when N₂O emissions are cumulated over longer periods, a model's ability to simulate the general dynamics of key driving factors controlling N₂O emissions is more important than the exact simulation of daily N₂O emission rates. Therefore, despite some uncertainties, our PSAM seems to be suitable to simulate cumulative N₂O emissions for balancing purposes.

4.4. Nitrogen Input Related Emission Factors

The sensitivity analysis of direct N₂O emissions with respect to continuously increased fertilizer N input showed a clear positive correlation and was best covered by quadratic functions (Table A2). These results reflect the fundamental context of available reactive N as a main driving factor for gaseous emissions, as well as the rather non-linear response reported from meta-studies globally [20,58] or under German conditions [59]. Other findings from simulation studies covered this as well [15,16]. For low-emitting sites and low N inputs, the N₂O response was nearly linear, but it was exponential at Merbitz due to higher site-specific emission potential. However, the EFs were predominantly much lower than the aggregated IPCC default value of 1%. Despite this generally low emission level, a site-specific response due to differences in pedoclimatic boundary conditions was obviously provided (Figure 8, Table 4). Gabrielle et al. [43] also highlighted this site-specific EF variation for wheat-cropped soils in France ranging from 0.07–0.3%, clearly

below the IPCC default value. The 10-year model simulation study of Leip et al. [21] also revealed large spatial variations of fertilizer-induced emissions and related EFs across European countries. However, their average resulting EF was on the level of the IPCC emission factor. It should be noted, that Leip et al. [21] calculated EFs, on average, of up to three crops, representing countries with typical agricultural structures. Accordingly, a direct comparison with our WOSR -pecific simulations for different sites across Germany is limited.

Our estimated EF_{200} and $EF_{N_{opt}}$ ranged from 0.16% to 0.65% at the investigated sites (Table 4) and were somewhat lower than those calculated by the global exponential model of Ruser et al. [22], including data from more sites as well as data from the meta-analysis by [59]. Thus, there were some sites included with clearly higher-observed N_2O emissions than were investigated in our research, leading to higher EFs. The more recent assessment for a Tier 2 regionalization of N_2O emission factors in Germany supports our findings, with a range of 0.38–0.92% and a mean value of 0.62% [23].

For the organic treatments with biogas digestate, calculated EFs were higher than the aggregated IPCC factor of 1% at two sites (Table 4). Even more discrepancies occurred when comparing the disaggregated IPCC factor or non-synthetic inputs in wet climates of 0.6%, as published in their refinements in 2019 [19]. One reason for the higher emissions from DIG might be that in addition to $180 \text{ kg NH}_4\text{-N ha}^{-1}$, on average $108 \text{ kg organic-bound N}$ was applied with the digestate [27], leading to real N-input levels of, on average, 260 kg N ha^{-1} (ammonia emissions were already subtracted). Nevertheless, our PSAM simulation of N_2O emissions from organic fertilization overestimated the observed N_2O emissions, especially at the high-emitting Merbitz site. Due to the lack of final evidence, a functional-relation study for organic fertilization was not feasible.

However, the reliable estimations of cumulative emissions, as well as the partial losses of applied N fertilizer from mineral sources (EF) based on long-term simulations, are useful tools in comparison to field measurements only. Especially for improvements in WOSR cropping sequences, the optimization of GHG balances, and the development of climate mitigation strategies, such site-specific evaluations are necessary. Particularly due the high GWP of N_2O , it is important to calibrate and evaluate such emission models very precisely.

5. Conclusions

Our newly integrated N_2O emission component was able to enhance an existing PSAM for predicting gaseous N losses. Specifically, for robust long-term cumulative assessments, the model was helpful for site-specific quantification of N_2O emissions from WOSR under high-intensity production conditions, which are typical for Germany. Improved daily flux dynamics must be a key aspect in further model revisions. Our three-year calibrated model enabled long-term simulations with historical weather data to derive reliable functional relations between fertilizer N input and direct N_2O emissions. Despite comparatively high typical fertilizer N inputs, simulated EFs were markedly below the IPCC standard value of 1%. In combination with previously published model components for indirect N_2O emissions from nitrate leaching and ammonia volatilization, a full set of gaseous N losses is now available to quantify climate impacts from WOSR cropping systems. This could help to improve quantifications as necessary for, e.g., bioenergy certifications, as well as to identify measures for climate-change mitigation in WOSR production. Moreover, future developments in regional and national climate inventories will need dynamic process-based simulation models for Tier 3 approaches. Further applications might also include scenario analysis with climate-change weather predictions to optimize future GHG balances in WOSR cropping sequences.

Supplementary Materials: The following supporting information can be downloaded at: <https://www.mdpi.com/article/10.3390/agriculture14010070/s1>, Table S1: Geographic locations of the study sites; Table S2: Dates of WOSR sowing and WOSR harvest for the five studied sites and the three investigated cropping periods; Table S3: Main characteristics of the digestates used at the five study sites; Table S4: Values of statistical criteria used to evaluate the SMN submodel relative to observations of SMN (0–30 cm); Table S5: Values of statistical criteria used to evaluate the simulation of soil water content by PSAM.

Author Contributions: Conceptualization: T.R. and H.K.; methodology: T.R., D.N., A.K., U.B. and H.K.; resources: D.N., A.K. and U.B.; supervision: H.K.; investigation: T.R.; validation: T.R.; visualization: T.R. and I.K.; writing—original draft: T.R. and I.K.; writing—review and editing: T.R., I.K., D.N. and H.K.; funding acquisition: H.K. All authors have read and agreed to the published version of the manuscript.

Funding: This work was funded by the German Federal Ministry of Food and Agriculture and managed by the Agency for Renewable Resources under grants 22403212, 22403312, 22403412, 22403512, 22403712, 22403812, and 22403912. We also thank the Union for the Promotion of Oil and Protein Plants, Germany, for its financial support.

Data Availability Statement: The field dataset is available online [60].

Acknowledgments: We thank all technical staff and students involved for their assiduous work in the field and the labs. Furthermore, we acknowledge financial support by DFG within the funding program ‘Open Access Publikationskosten’.

Conflicts of Interest: The authors declare no conflict of interest.

Appendix A

Additional Formulas during Nitrification Processes

$$f_{abiot_{nit}} = f(W)_{nit} \cdot f(T)_{nit} \quad (A1)$$

where $f(W)_{nit}$ and $f(T)_{nit}$ represent water and temperature impacts:

$$f(W)_{nit} = \begin{cases} 1 - \frac{(1.5-pF)}{1.5} & pF < 1.5 \\ 1 & 1.5 \leq pF < 2.5 \\ 1 - 0.4 \cdot (pF - 2.5) & 2.5 \leq pF < 5 \\ 0 & pF \geq 5 \end{cases} \quad (A2)$$

where pF describes soil matric potential as the decadic logarithm of its absolute value in hPa.

$$f(T)_{nit} = \begin{cases} 0 & T \leq 2 \text{ }^\circ\text{C} \\ 0.15 \cdot (T - 2) & 2 \text{ }^\circ\text{C} < T \leq 6 \text{ }^\circ\text{C} \\ 0.1 \cdot T & 6 \text{ }^\circ\text{C} < T \leq 20 \text{ }^\circ\text{C} \\ e^{0.47 - 0.027 \cdot T + 0.00193 \cdot T^2} & 20 \text{ }^\circ\text{C} < T \leq 28 \text{ }^\circ\text{C} \\ e^{0.47 - 0.027 \cdot 28 + 0.00193 \cdot 28^2} & T > 28 \text{ }^\circ\text{C} \end{cases} \quad (A3)$$

where T describes the soil temperature in $^\circ\text{C}$.

$$R_{NO_x/N_2O} = e^{-3.79 \cdot WFPS + 2.73} \quad (A4)$$

where $WFPS$ represents water-filled pore space [$\text{cm}^3 \text{ cm}^{-3}$].

Additional Formulas during Denitrification Processes

$$k_{pot_{den}} = k_{den} \cdot CO_2 \text{ flux} \quad (A5)$$

$$f_{abiot_{den}} = f(W)_{den} \cdot f(T)_{den} \quad (A6)$$

where $f(W)_{den}$ and $f(T)_{den}$ represent water and temperature impacts:

$$f(W)_{den} = \min\left(1, \max\left(0, \frac{WC - WC(WFPS_{crit_den})}{WC_{sat} - WC(WFPS_{crit_den})}\right)\right) \quad (A7)$$

where water content WC is calculated from water-filled pore space $WFPS$, taking soil texture dependent saturated water content WC_{sat} into account:

$$WC(WFPS) = WFPS \cdot WC_{sat} \quad (A8)$$

$$f(T)_{den} = 0.1 \cdot e^{0.046 \cdot T} \quad (A9)$$

$$R_{N_2/N_2O} = \max\left(0.16 \cdot k_1, k_1 \cdot \exp\left(-0.8 \cdot \frac{NO_3}{CO_2 - flux}\right)\right) \cdot \max(0.1, 1.5 \cdot WFPS - 0.32) \quad (A10)$$

where k_1 is the parameter controlling the maximum value of the N_2/N_2O ratio curve:

$$k_1 = \max(1.7, 38.4 - 350 \cdot D_{FC}) \quad (A11)$$

where D_{FC} represents the soil gas diffusion at field capacity, calculated after Millington and Quirk (1961) in Kristensen et al. [61]

$$D_{FC} = \frac{\varepsilon^{10}}{\Phi^2} \quad (A12)$$

where Φ is the total porosity [$\text{cm}^3 \text{cm}^{-3}$] and ε is the air-filled pore space at field capacity [$\text{cm}^3 \text{cm}^{-3}$].

Table A1. Parametrization details of the N_2O -emission processes.

Parameter	Unit	Value	Source/Fitting
CN_{DPM}	-	6	[39]
CN_{RPM}	-	150	assumption
CN_{BIOM}	-	8	[39]
CN_{SOM}	-	10	[39]
ε_{DPM}	-	0.4	
ε_{RPM}	-	0.3	[39]
ε_{BIOM}	-	1	
ε_{SOM}	-	0.2	
$k_{DPM \rightarrow BIOM}$	day ⁻¹	0.07	
$k_{RPM \rightarrow BIOM}$	day ⁻¹	0.007	[34]
$k_{BIOM \rightarrow SOM}$	day ⁻¹	0.01	
$k_{SOM \rightarrow BIOM}$	day ⁻¹	Berge: 0.00037 Dedelow: 0.00090 Hohenschulen: 0.00037 Ihinger Hof: 0.00050 Merbitz: 0.00055	fitted to $SMN_{measured}$
Min_{eff}	-	Berge: 1.0 Dedelow: 1.5 Hohenschulen: 1.0 Ihinger Hof: 1.0 Merbitz: 1.5	fitted to $SMN_{measured}$
$fr_{-n-loss}$	-	0.0157	
k_{nit}	day ⁻¹	0.18	fitted to $NH_4-N_{measured}$
k_{den}	day ⁻¹	1.9	fitted to $N_2O_{measured}$
K_m	-	26	[36]

Table A1. Cont.

Parameter	Unit	Value	Source/Fitting
$WFPS_{crit_den}$	[%]	Berge: 0.90 Dedelow: 0.85 Hohenschulen: 0.80 Ihinger Hof: 0.95 Merbitz: 0.87	fitted to N_2O measured

Table A2. Site-specific equations and coefficients of determination for the estimated regression lines between N-induced N_2O emissions and mineral N input. N_2O emissions as long-term medians of respective mineral N-input level from long-term simulations.

Site	x = Mineral N input [$kg\ N\ ha^{-1}$] y = N_2O Emission [$kg\ N_2O-N\ ha^{-1}$]	R^2
Berge	$y = 1.163 \cdot 10^{-6} x^2 + 1.465 \cdot 10^{-3} x - 9.575 \cdot 10^{-3}$	0.90
Dedelow	$y = 1.343 \cdot 10^{-6} x^2 + 1.397 \cdot 10^{-3} x - 1.033 \cdot 10^{-2}$	0.87
Hohenschulen	$y = 3.687 \cdot 10^{-6} x^2 + 1.083 \cdot 10^{-3} x + 4.036 \cdot 10^{-3}$	0.82
Ihinger Hof	$y = 6.076 \cdot 10^{-6} x^2 + 1.952 \cdot 10^{-3} x + 8.347 \cdot 10^{-3}$	0.84
Merbitz	$y = 2.876 \cdot 10^{-5} x^2 + 9.143 \cdot 10^{-4} x - 3.647 \cdot 10^{-2}$	0.61

Table A3. Derived economic optimal N fertilizer input (N_{opt}) and corresponding yield ($Y_{N_{opt}}$) from quadratic response functions at the five study sites.

Site	N_{opt} [$kg\ N\ ha^{-1}$]	$Y_{N_{opt}}$ [$t\ ha^{-1}$]
Berge	191	3.62
Dedelow	196	3.92
Hohenschulen	222	4.54
Ihinger Hof	222	4.21
Merbitz	201	4.33

References

- IPCC. AR6 WG1; IPCC: Geneva, Switzerland, 2021.
- Tian, H.; Xu, R.; Canadell, J.G.; Thompson, R.L.; Winiwarter, W.; Suntharalingam, P.; Davidson, E.A.; Ciais, P.; Jackson, R.B.; Janssens-maenhout, G.; et al. A comprehensive quantification of global nitrous oxide sources and sinks. *Nature* **2020**, *586*, 248–256. [\[CrossRef\]](#)
- Conrad, R. Soil microorganisms as controllers of atmospheric trace gases (H_2 , CO, CH_4 , OCS, N_2O , and NO). *Microbiol. Rev.* **1996**, *60*, 609–640. [\[CrossRef\]](#)
- Köster, J.R.; Cárdenas, L.; Senbayram, M.; Bol, R.; Well, R.; Butler, M.; Mühling, K.H.; Dittert, K. Rapid shift from denitrification to nitrification in soil after biogas residue application as indicated by nitrous oxide isotopomers. *Soil Biol. Biochem.* **2011**, *43*, 1671–1677. [\[CrossRef\]](#)
- Signor, D.; Cerri, C.E.D. Nitrous oxide emissions in agricultural soils: A review. *Pesqui. Agropecuária Trop.* **2013**, *43*, 322–338. [\[CrossRef\]](#)
- Prosser, J.I. NITROGEN IN SOILS | Nitrification. In *Encyclopedia of Soils in the Environment*; Elsevier: Amsterdam, The Netherlands, 2005; pp. 31–39, ISBN 9780123485304.
- Butterbach-Bahl, K.; Baggs, E.M.; Dannenmann, M.; Kiese, R.; Zechmeister-Boltenstern, S. Nitrous oxide emissions from soils: How well do we understand the processes and their controls? *Phil. Trans. R. Soc. B* **2013**, *368*, 20130122. [\[CrossRef\]](#)
- Hénault, C.; Germon, J.C. NEMIS, a predictive model of denitrification on the field scale. *Eur. J. Soil Sci.* **2000**, *51*, 257–270. [\[CrossRef\]](#)
- Weier, K.L.; Doran, J.W.; Power, J.F.; Walters, D.T. Denitrification and the Dinitrogen/Nitrous Oxide Ratio as Affected by Soil Water, Available Carbon, and Nitrate. *Soil Sci. Soc. Am. J.* **1993**, *57*, 66–72. [\[CrossRef\]](#)
- Chen, C.; Chen, D.; Pan, J.; Lam, S.K. Analysis of factors controlling soil N_2O emission by principal component and path analysis method. *Environ. Earth Sci.* **2014**, *72*, 1511–1517. [\[CrossRef\]](#)
- Zumft, W.G. Cell biology and molecular basis of denitrification. *Microbiol. Mol. Biol. Rev.* **1997**, *61*, 533–616. [\[CrossRef\]](#)
- Ruser, R.; Flessa, H.; Russow, R.; Schmidt, G.; Buegger, F.; Munch, J.C. Emission of N_2O , N_2 and CO_2 from soil fertilized with nitrate: Effect of compaction, soil moisture and rewetting. *Soil Biol. Biochem.* **2006**, *38*, 263–274. [\[CrossRef\]](#)

13. Mosier, A.R.; Doran, J.W.; Freney, J.R. Managing soil denitrification. *J. Soil Water Conserv.* **2002**, *57*, 505–512.
14. Rochette, P.; Eriksen-Hamel, N.S. Chamber Measurements of Soil Nitrous Oxide Flux: Are Absolute Values Reliable? *Soil Sci. Soc. Am. J.* **2008**, *72*, 331–342. [[CrossRef](#)]
15. Li, Y.; Barton, L.; Chen, D. Simulating response of N₂O emissions to fertiliser N application and climatic variability from a rain-fed and wheat-cropped soil in Western Australia. *J. Sci. Food Agric.* **2012**, *92*, 1130–1143. [[CrossRef](#)]
16. Goglio, P.; Colnenne-David, C.; Laville, P.; Doré, T.; Gabrielle, B. 29% N₂O emission reduction from a modelled low-greenhouse gas cropping system during 2009–2011. *Environ. Chem. Lett.* **2013**, *11*, 143–149. [[CrossRef](#)]
17. Parton, W.J.; Mosier, A.R.; Ojima, D.S.; Valentine, D.W.; Schimel, D.S.; Weier, K.; Kulmala, A.E. Generalized model for N₂ and N₂O production from nitrification and denitrification. *Glob. Biogeochem. Cycles* **1996**, *10*, 401–412. [[CrossRef](#)]
18. IPCC. Chapter 11: N₂O emissions from managed soils, and CO₂ emissions from lime and urea application. In *IPCC Guidelines for National Greenhouse Gas Inventories*; IPCC: Geneva, Switzerland, 2006; pp. 11.1–11.54.
19. IPCC. N₂O Emissions from Managed Soils, and CO₂ Emissions from Lime and Urea Application. In *2019 Refinement to the 2006 IPCC Guidelines for National Greenhouse Gas Inventories*; IPCC: Geneva, Switzerland, 2019; pp. 1–48, ISBN 4887880324.
20. Shcherbak, I.; Millar, N.; Robertson, G.P. Global metaanalysis of the nonlinear response of soil nitrous oxide (N₂O) emissions to fertilizer nitrogen. *Proc. Natl. Acad. Sci. USA* **2014**, *111*, 9199–9204. [[CrossRef](#)]
21. Leip, A.; Busto, M.; Winiwarter, W. Developing spatially stratified N₂O emission factors for Europe. *Environ. Pollut.* **2011**, *159*, 3223–3232. [[CrossRef](#)]
22. Ruser, R.; Fuß, R.; Andres, M.; Hegewald, H.; Kesenheimer, K.; Köbke, S.; Rübiger, T.; Quinones, T.S.; Augustin, J.; Christen, O.; et al. Nitrous oxide emissions from winter oilseed rape cultivation. *Agric. Ecosyst. Environ.* **2017**, *249*, 57–69. [[CrossRef](#)]
23. Mathivanan, G.P.; Eysholdt, M.; Zinnbauer, M.; Rösemann, C.; Fuß, R. New N₂O emission factors for crop residues and fertiliser inputs to agricultural soils in Germany. *Agric. Ecosyst. Environ.* **2021**, *322*, 107640. [[CrossRef](#)]
24. Heinen, M. Simplified denitrification models: Overview and properties. *Geoderma* **2005**, *133*, 444–463. [[CrossRef](#)]
25. DESTATIS Regional Database Germany Verfügbar Unter. Available online: <https://www.regionalstatistik.de/genesis/online> (accessed on 21 November 2023).
26. Fuss, R.; Hueppi, R.; Pedersen, A.R. Package ‘Gasfluxes’. 2019. Available online: <https://cran.r-project.org/web/packages/gasfluxes/gasfluxes.pdf> (accessed on 29 November 2023).
27. Rübiger, T.; Andres, M.; Hegewald, H.; Kesenheimer, K.; Köbke, S.; Quinones, T.S.; Böttcher, U.; Kage, H. Indirect nitrous oxide emissions from oilseed rape cropping systems by NH₃ volatilization and nitrate leaching as affected by nitrogen source, N rate and site conditions. *Eur. J. Agron.* **2020**, *116*, 126039. [[CrossRef](#)]
28. Böttcher, U.; Weymann, W.; Pullens, J.W.M.; Olesen, J.E.; Kage, H. Development and evaluation of HUME-OSR: A dynamic crop growth model for winter oilseed rape. *Field Crops Res.* **2020**, *246*, 107679. [[CrossRef](#)]
29. Weymann, W. *Model-Base Analysis of Weather, Soil and Management Effects on Yield Formation of Winter Oilseed Rape*; Christian-Albrechts-Universität zu Kiel: Kiel, Germany, 2015.
30. Ratjen, A.M.; Kage, H. Forecasting yield via reference- and scenario calculations. *Comput. Electron. Agric.* **2015**, *114*, 212–220. [[CrossRef](#)]
31. Kage, H.; Stützel, H. HUME: An object oriented component library for generic modular modelling of dynamic systems. *Model. Crop. Syst.* **1999**, 2–3.
32. Kage, H.; Alt, C.; Stützel, H. Aspects of nitrogen use efficiency of cauliflower I. A simulation modelling based analysis of nitrogen availability under field conditions. *J. Agric. Sci.* **2003**, *141*, 1–16. [[CrossRef](#)]
33. Zhou, Z.; Zheng, X.; Xie, B.; Han, S.; Liu, C. A process-based model of N₂O emission from a rice-winter wheat rotation agro-ecosystem: Structure, validation and sensitivity. *Adv. Atmos. Sci.* **2010**, *27*, 137–150. [[CrossRef](#)]
34. Hansen, S.; Jensen, H.; NE, N.; Svendsen, H. *NPo-Research, A10: DAISY: Soil Plant Atmosphere System Model*; Miljøstyrelsen: Copenhagen, Denmark, 1990.
35. Thorburn, P.J.; Biggs, J.S.; Collins, K.; Probert, M.E. Using the APSIM model to estimate nitrous oxide emissions from diverse Australian sugarcane production systems. *Agric. Ecosyst. Environ.* **2010**, *136*, 343–350. [[CrossRef](#)]
36. Del Grosso, S.J.; Parton, W.J.; Mosier, A.R.; Ojima, D.S.; Kulmala, A.E.; Phongpan, S. General model for N₂O and N₂ gas emissions from soils due to denitrification. *Global Biogeochem. Cycles* **2000**, *14*, 1045–1060. [[CrossRef](#)]
37. van Genuchten, M.T. A Closed-form Equation for Predicting the Hydraulic Conductivity of Unsaturated Soils. *Soil Sci. Soc. Am. J.* **1980**, *44*, 892–898. [[CrossRef](#)]
38. Henke, J.; Böttcher, U.; Neukam, D.; Sieling, K.; Kage, H. Evaluation of different agronomic strategies to reduce nitrate leaching after winter oilseed rape (*Brassica napus* L.) using a simulation model. *Nutr. Cycl. Agroecosyst.* **2008**, *82*, 299–314. [[CrossRef](#)]
39. Verberne, E.L.J.; Hassink, J.; de Willigen, P.; Groot, J.J.R.; van Veen, J.A. Modelling organic matter dynamics in different soils. *Neth. J. Agric. Sci.* **1990**, *38*, 221–238. [[CrossRef](#)]
40. R Core Team. *R: A Language and Environment for Statistical Computing R. Foundation for Statistical Computing*; Version 4.1.2; R Core Team: Vienna, Austria, 2021.
41. Neeteson, J.J.; Wadman, W.P. Assessment of economically optimum application rates of fertilizer N on the basis of response curves. *Fertil. Res.* **1987**, *12*, 37–52. [[CrossRef](#)]
42. Dhakal, C.; Lange, K. Crop yield response functions in nutrient application: A review. *Agron. J.* **2021**, *113*, 5222–5234. [[CrossRef](#)]

43. Gabrielle, B.; Laville, P.; Duval, O.; Nicoulaud, B.; Germon, J.C.; Hénault, C. Process-based modeling of nitrous oxide emissions from wheat-cropped soils at the subregional scale. *Global Biogeochem. Cycles* **2006**, *20*, GB4018. [[CrossRef](#)]
44. Yuan, F.; Meixner, T.; Fenn, M.E.; Šimůnek, J. Impact of transient soil water simulation to estimated nitrogen leaching and emission at high- and low-deposition forest sites in Southern California. *J. Geophys. Res.* **2011**, *116*, G03040. [[CrossRef](#)]
45. Cui, J.; Li, C.; Sun, G.; Trettin, C. Linkage of MIKE SHE to Wetland-DNDC for carbon budgeting and anaerobic biogeochemistry simulation. *Biogeochemistry* **2005**, *72*, 147–167. [[CrossRef](#)]
46. Myrsgiotis, V.; Williams, M.; Rees, R.M.; Topp, C.F.E. Estimating the soil N₂O emission intensity of croplands in northwest Europe. *Biogeosciences* **2019**, *16*, 1641–1655. [[CrossRef](#)]
47. Li, X.; Yeluripati, J.; Jones, E.O.; Uchida, Y.; Hatano, R. Hierarchical Bayesian calibration of nitrous oxide (N₂O) and nitrogen monoxide (NO) flux module of an agro-ecosystem model: ECOSSE. *Ecol. Modell.* **2015**, *316*, 14–27. [[CrossRef](#)]
48. Smith, W.; Grant, B.; Qi, Z.; He, W.; VanderZaag, A.; Drury, C.F.; Helmers, M. Development of the DNDC model to improve soil hydrology and incorporate mechanistic tile drainage: A comparative analysis with RZWQM2. *Environ. Model. Softw.* **2020**, *123*, 104577. [[CrossRef](#)]
49. Mielenz, H.; Thorburn, P.J.; Scheer, C.; De Antoni Migliorati, M.; Grace, P.R.; Bell, M.J. Opportunities for mitigating nitrous oxide emissions in subtropical cereal and fiber cropping systems: A simulation study. *Agric. Ecosyst. Environ.* **2016**, *218*, 11–27. [[CrossRef](#)]
50. Guest, G.; Kröbel, R.; Grant, B.; Smith, W.; Sansoulet, J.; Pattey, E.; Desjardins, R.; Jégo, G.; Tremblay, N.; Tremblay, G. Model comparison of soil processes in eastern Canada using DayCent, DNDC and STICS. *Nutr. Cycl. Agroecosyst.* **2017**, *109*, 211–232. [[CrossRef](#)]
51. Groffman, P.M.; Tiedje, J.M. Relationships between denitrification, CO₂ production and air-filled porosity in soils of different texture and drainage. *Soil Biol. Biochem.* **1991**, *23*, 299–302. [[CrossRef](#)]
52. Velthof, G.L.; Kuikman, P.J.; Oenema, O. Nitrous oxide emission from animal manures applied to soil under controlled conditions. *Biol. Fertil. Soils* **2003**, *37*, 221–230. [[CrossRef](#)]
53. Chadwick, D.R.; Pain, B.F.; Brookman, S.K.E. Nitrous Oxide and Methane Emissions following Application of Animal Manures to Grassland. *J. Environ. Qual.* **2000**, *29*, 277–287. [[CrossRef](#)]
54. Li, C.; Aber, J.; Stange, F.; Butterbach-Bahl, K.; Papen, H. A process-oriented model of N₂O and NO emissions from forest soils: 1. Model development. *J. Geophys. Res. Atmos.* **2000**, *105*, 4369–4384. [[CrossRef](#)]
55. Yang, Q.; Zhang, X.; Abrahama, M.; Del grosso, S.; Robertson, G.P.; Chen, J. Enhancing the soil and water assessment tool model for simulating N₂O emissions of three agricultural systems. *Ecosyst. Health Sustain.* **2017**, *3*, 11879067. [[CrossRef](#)]
56. Bell, M.J.; Jones, E.; Smith, J.; Smith, P.; Yeluripati, J.; Augustin, J.; Juszczak, R.; Olejnik, J.; Sommer, M. Simulation of soil nitrogen, nitrous oxide emissions and mitigation scenarios at 3 European cropland sites using the ECOSSE model. *Nutr. Cycl. Agroecosyst.* **2012**, *92*, 161–181. [[CrossRef](#)]
57. Molina-Herrera, S.; Haas, E.; Klatt, S.; Kraus, D.; Augustin, J.; Magliulo, V.; Tallec, T.; Ceschia, E.; Ammann, C.; Loubet, B.; et al. A modeling study on mitigation of N₂O emissions and NO₃ leaching at different agricultural sites across Europe using LandscapeDNDC. *Sci. Total Environ.* **2016**, *553*, 128–140. [[CrossRef](#)]
58. Kim, D.G.; Hernandez-Ramirez, G.; Giltrap, D. Linear and nonlinear dependency of direct nitrous oxide emissions on fertilizer nitrogen input: A meta-analysis. *Agric. Ecosyst. Environ.* **2013**, *168*, 53–65. [[CrossRef](#)]
59. Walter, K.; Don, A.; Fuß, R.; Kern, J.; Drewer, J.; Flessa, H. Direct nitrous oxide emissions from oilseed rape cropping—A meta-analysis. *GCB Bioenergy* **2015**, *7*, 1260–1271. [[CrossRef](#)]
60. Mallast, J.; Stichnothe, H.; Flessa, H.; Fuß, R.; Lucas-Moffat, A.M.; Petersen-Schlapkohl, U.; Augustin, J.; Hagemann, U.; Kesenheimer, K.; Ruser, R.; et al. Multi-variable experimental data set of agronomic data and gaseous soil emissions from maize, oilseed rape and other energy crops at eight sites in Germany. *Open Data J. Agric. Res.* **2021**, *7*, 11–19. [[CrossRef](#)]
61. Kristensen, A.H.; Thorbjørn, A.; Jensen, M.P.; Pedersen, M. Gas-phase diffusivity and tortuosity of structured soils. *J. Contam. Hydrol.* **2010**, *115*, 26–33. [[CrossRef](#)] [[PubMed](#)]

Disclaimer/Publisher’s Note: The statements, opinions and data contained in all publications are solely those of the individual author(s) and contributor(s) and not of MDPI and/or the editor(s). MDPI and/or the editor(s) disclaim responsibility for any injury to people or property resulting from any ideas, methods, instructions or products referred to in the content.